Journal of Solid State Chemistry **166,** 237–244 (2002)
doi:10.1006/jssc.2002.9596, available online at http://www.idealibrary.com on IDEAL®

# Conductivity and Structural Investigations in Lacunary $Pb_6Ca_2Li_2(PO_4)_6$ Apatite

Thouraya Naddari,* Jean-Michel Savariault,†,[1] Hafed El Feki,* Philippe Salles,† and Abdelhamid Ben Salah*

*Laboratoire des Sciences des Matériaux et Environnement, Faculté des Sciences de SFAX, BP 802, 3018 SFAX, Tunisia; †Centre d'Elaboration de Matériaux et d'Etudes Structurales, 29 rue J. Marvig, BP 4347, 31055 Toulouse Cedex 4, France

Received December 12, 2001; received in revised form March 11, 2002; accepted March 22, 2002

**Prismatic crystals of $Pb_6Li_2Ca_2(PO_4)_6$ were obtained by solid-state reaction. They were characterized by IR spectroscopy and chemical analyses. The structure as determined by X-ray diffraction study on single crystal revealed that the compound is isostructural to the hexagonal phase $Pb_8Na_2(PO_4)_6$. Crystal data for $Pb_6Li_2Ca_2(PO_4)_6$: space group $P63/m$ (No. 176), $a = b = 9.6790(15)$ Å, $c = 7.1130(7)$, $Z = 1$, $R = 0.039$. In the compound, lithium was found to preferentially occupy the site (I) and the structure is stabilized by interactions between electron lone pairs of lead (II) ions. Electrical conductivity measured in a wide range of temperature is governed by a hopping mechanism of Li ions in tunnels.** © 2002 Elsevier Science (USA)

***Key Words:*** **lead apatite; single crystals; lithium; IR spectroscopy; structure; electrical conductivity.**

## INTRODUCTION

Apatite minerals crystallize in the fluorapatite ($Ca_5(PO_4)_3F$) type structure. Their general formula is written as $M(II)_3M(I)_2(XO_4)_3Y$, where $M(I)$ and $M(II)$ metal ions occupy large sites ($4f$) and ($6h$) with nine and seven coordination, respectively. $X$ is a four-coordinated tetrahedral site, and $Y$ is an anion site. The $Y$ sites lie in the center of channels which are parallel to the $c$-axis. These channels also contain the $M(II)$ sites, which form equilateral triangles that alternate in orientation and are stacked in the $c$-direction. Apatites are prone to extensive ionic substitutions (1). Divalent cations such as $Sr^{2+}$, $Ba^{2+}$, $Pb^{2+}$ and $Cd^{2+}$ can be used as substitutes for $Ca^{2+}$ on the $M$ sites. Substitutions for fluoride involve electronegative anions such as $Cl^-$ or $OH^-$. The $X$ site is occupied by elements that form small tetrahedral oxyanions, the most common being $PO_4^{3-}$, $AsO_4^{3-}$, $VO_4^{3-}$, $SO_4^{2-}$ or $SiO_4^{4-}$ (2–4).

Because of these various substitutions, minerals that belong to the apatite family are well-known for their compositional variations. This fact has initiated many studies for exploring the possibility of synthesizing solid solutions based on apatite structure. Besides their biological importance (5, 6), apatite-type compounds were studied extensively for potential use as fluorescent lamp phosphors (7, 8) or laser hosts material (9–12).

Lead in apatites has drawn substantial attention from two points of view. First, lead is known as a "bone seeker", in that it accumulates in bones and teeth. Second, it may contribute to deviation from the general formula of apatites.

Apatites which deviate from the ideal formula $Me_5(XO_4)_3Y$ would require charge compensation brought by various substitutions. Nevertheless, the only system, where compounds with the apatite structure could be prepared without anion $Y$, is the lead system (13).

Because of the mobility of $Me$ or $Y$ ions in such compounds, investigations on electrical measurements were performed. Several authors have established a correlation between structural properties and ionic conductivities (14–20). Comparisons of electrical properties of fluorapatite and hydroxyapatite electrolytes show that the behavior with temperature of apatite containing lead differs from other apatites, which is attributed to the interaction of Pb–Y in the tunnel. Moreover, fluorapatite compounds are found to be better ionic conductors than the hydroxyapatite (18).

The study of cationic conductivity of the $Pb_8K_{2-x}Na_x(PO_4)_6$ system shows that the variation of the ionic conductivity versus the sodium content is related to the change of the polarizing character of the metals and the variation of size of the apatite tunnels (15).

Although investigations of apatites having vacancies in the $Y$ anion sites with the general formula $Pb_8M_2(XO_4)_6$

[1] To whom correspondence should be addressed. Fax: (33) 5-62-25-79-99. E-mail: savariau@cemes.fr.



0022-4596/02 $35.00
© 2002 Elsevier Science (USA)
All rights reserved.

($M$: monovalent cation) have been studied by several authors (5, 21–26), there is no study reported on the synthesis, characterization and crystal structure of the lacunate lead apatite, partially substituted for calcium and lithium, of formula $Pb_6Ca_2Li_2(PO_4)_6$ (named LCPbAp in the study). In this paper, we present the synthesis, the structure determination and the conductivity study of this compound.

## EXPERIMENTAL

### *Synthesis and Characterization*

LCPbAp crystals were grown during a solid-state reaction involving reagent-grade $Li_2CO_3$, $(NH_4)_2HPO_4$, $CaCO_3$ and PbO powders. Thoroughly mixed starting materials in the appropriate stoichiometry were heated at 800°C in air for 12 h and subsequently at 900°C for 12 h. The crystals obtained were of hexagonal prismatic shape. The chemical formula was determined from chemical analysis (27) and confirmed by crystal structure refinement. The single crystals studied correspond to the composition $Pb_{6.12}Ca_{1.90}Li_{1.96}(PO_4)_6$.

A pellet made of 1.5 mg apatite powder mixed with 300 mg KBr powder of spectroscopic grade was used for infrared measurement. The spectrum was recorded in the range 4000–400 $cm^{-1}$ with a JASCO FT/IR 420 spectrometer.

### *Intensity Data Collection and Refinement*

The X-ray single-crystal study was performed using a Kappa CCD diffractometer, with a graphite monochromatized Mo$K\alpha_1$ radiation ($\lambda = 0.71069$ Å). It revealed LCPbAp to be hexagonal. The data pertinent to crystal and X-ray measurement are given in Table 1. Atomic scattering factors were those of the refinement program SHELX 97 (28, 29). The structure was successfully determined in space group $P6_3/m$ (No. 176). Full matrix refinement including anisotropic thermal displacement parameters of every atom converged to a final $R$ value of 0.039.

### *Electrical Properties*

The electrical conductivity was studied using Electrochemical Impedance Spectroscopy (EIS) and measurements were performed on an HP 4192 A impedance analyzer. The signal frequency ranged from 100 Hz to 13 MHz.The sample was pressed as a pellet under 2 ton/$cm^2$ and sintered at 1000 K. Its density was about 96%. Electrodes were prepared by painting Pt paste on both sides of the sintered pellet surfaces and subsequently annealing at 873 K.

**TABLE 1**
**Crystal Data and Structure Refinement Information of LCPbAp Compound**

| | | |
|---|---|---|
| *I— Crystal data* | | |
| Formula | | $Pb_{6.12}Ca_{1.90}Li_{1.96}(PO_4)_6$ |
| Formula weight | | 1907.00 |
| System: Hexagonal | | Space group: $P6_3/m$ |
| $a$ =9.6790(15) Å | | $c$ =7.1130(7) Å |
| $Z = 1$ | | $V$ =577.09(14) Å$^3$ |
| $\rho_{cal}$ = 5.48 (g $cm^{-3}$) | | $F(000)$ = 820.0 |
| Linear absorption factor ($mm^{-1}$) | | $\mu$(Mo$K\alpha$) = 44.57 |
| Morphology: Prismatic | | Colorless |
| Crystal size | | $0.1 \times 0.1 \times 0.12$ $mm^3$ |
| *II—Intensity measurements* | | |
| Temperature | 293(2) K | Wavelength Mo$K\alpha$ (0.71069 Å) |
| 2-$\theta$ range | 39.81° | |
| Measurement area $h, k, l$ | | $-9 \le h \le 6$, $-8 \le k \le 6$, $-6 \le l \le 6$ |
| Total reflections | 917 | $R_{int}$ = 0.095 |
| *III— Structure determination* | | |
| Numerical absorption correction | | $T_{min}$ = 0.039, $T_{max}$ = 0.091 |
| Refinement method | | Full-matrix least squares on $F^2$ , SHELXL |
| Unique reflections with $I > 4\sigma(I)$ | | 155 |
| Refined parameters | 43 | Residual electronic density –1.18, 1.75 e/Å$^3$ |
| Agreement factors | $R$ =0.039 | w$R_2$ = 0.082 |
| Goodness of fit | $s$ =1.16 | |

## RESULTS AND DISCUSSIONS

### *IR Spectroscopy*

The infrared spectrum of LCPbAp is shown in Fig. 1. A comparison to the modes of frequencies observed in similar compounds allows the assignment of the IR spectra (25, 26, 30). Internal vibrations of $PO_4$ tetrahedra reduced to four IR active vibrational frequencies, corresponding to two stretching modes $\gamma_1$ and $\gamma_3$ and two bending modes $\gamma_2$ and $\gamma_4$ . These vibrations are expected in the 1200–800 and 600–350 $cm^{-1}$ ranges, respectively. Since the frequencies of the $\gamma_1$ and $\gamma_3$ stretching vibrations of the $PO_4$ anion are rather

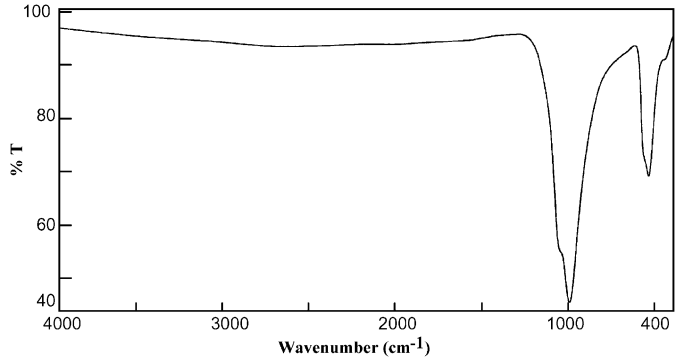


**FIG. 1.** Infrared absorption spectrum of $Pb_6Ca_2Li_2(PO_4)_6$ compound.

**TABLE 2**
**Final Least-Squares Atomic Parameters with Estimated Standard Deviations for LCPbAp Compound**

| Atom | Occupancy | $x$ | $y$ | $z$ | $U_{eq}$ (Å$^2$) |
|---|---|---|---|---|---|
| Pb(II) | 0.415(4) | 0.2510(2) | 0.0040(2) | $\frac{1}{4}$ | 0.013(1) |
| Ca(II) | 0.085(4) | 0.2510(2) | 0.0040(2) | $\frac{1}{4}$ | 0.013(1) |
| Pb(I) | 0.095(17) | $\frac{2}{3}$ | $\frac{1}{3}$ | −0.0084(7) | 0.008(3) |
| Li(I) | 0.163(4) | $\frac{2}{3}$ | $\frac{1}{3}$ | −0.0084(7) | 0.008(3) |
| Ca(I) | 0.073(4) | $\frac{2}{3}$ | $\frac{1}{3}$ | −0.0084(7) | 0.008(3) |
| P | 0.5 | 0.4112(9) | 0.3842(9) | $\frac{1}{4}$ | 0.006(6) |
| O3 | 1 | 0.358(2) | 0.273(2) | 0.077(2) | 0.03(1) |
| O2 | 0.5 | 0.352(2) | 0.506(2) | $\frac{1}{4}$ | 0.03(2) |
| O1 | 0.5 | 0.596(7) | 0.475(5) | $\frac{1}{4}$ | 0.024(2) |

*Note.* $U_{eq} = \frac{1}{3}\sum_i\sum_j U(i,j)a^*_i a^*_j a_i a_j$.

similar (30), the broadband at about 1043 cm$^{-1}$ can be assigned to the asymmetric $\gamma_3$ vibration, superimposed to the symmetric stretching vibration $\gamma_1$. On the other hand, the lines observed in the region 545 cm$^{-1}$ are associated to the $\gamma_4$ and $\gamma_2$ vibrations.

No vibration characteristics of OH groups can be observed in the 3500–4000 cm$^{-1}$ range (30). This confirms that the present apatite does not contain hydroxyl groups or intercalated water in tunnels.

## *Structural Properties*

Final coordinates and isotropic thermal parameters are given in Table 2. Table 3 presents all anisotropic thermal displacement parameters. Selected interatomic distances and angles are listed in Table 4. Figure 2. shows a perspective drawing of the LCPbAp structure. The mean feature of this structure is the coexistence of three different cations, $Pb^{2+}$, $Ca^{2+}$, $Li^+$, in the same crystal with the ratio 6.12/1.90/1.96, respectively.

A comparison of this structure with the structure of $Pb_8Na_2(PO_4)_6$ or $Pb_6Ca_2Na_2(PO_4)_6$ (24, 31), reveales a great similarity in atomic arrangement. This structure is of the $M^1_2Pb_8(XO_4)_6$ type which is an anionic lacunary apatite (3, 5, 21–23).

The $PO_4$ ion exhibits a significant deformation. The three angles around the P–O2 bond are significantly larger than the three other angles (O2–P–O1 and O2–P–O3 average 112°(4), O1–P–O3 and O3–P–O3 average 106.3°(3)). A similar discrepancy (110°(5) and 108.5°(1) is already observed in hydroxyapatite (32), but the divergence (1.5°) is smaller than that in the present compound (5.7°). Such variation can be attributed to lead (II) and its electron lone pair (LP).

Site (I) is occupied by 0.88 $Ca^{2+}$, 1.96 $Li^+$ and 1.148 $Pb^{2+}$ (Table 2). These cations are coordinated to nine oxide anions forming a tricapped trigonal prism. We observe that metal(I) is shifted 0.060(5) Å from the center of the prism, while in hydroxyapatite it is only 0.017(2) Å (32). Such an increase in shift leads to a short $M$(I)–$M$(I) distance (3.433(4) Å and a longer one (3.680(1) Å) (Table 3), which can be explained assuming lead LP pointing to each other every second Pb(I)–Pb(I) interval (Fig. 3). But due to the diffraction phenomenon, the shift of metal out of the centre corresponds to a weighting average of Pb and Ca shift (Li shift is assumed to be equal to Ca shift). The weighting is due to the occupancy number and the scattering factor (the number of electrons) of each atom. Using the Ca shift observed in hydroxyapatite, a simple

**TABLE 3**
**Final Anisotropic Displacement Thermal Parameters (Å$^2$) with Estimated Standard Deviations for LCPbAp Compound**

| Atom | $U$(1,1) | $U$(2,2) | $U$(3,3) | $U$(1,2) | $U$(1,3) | $U$(2,3) |
|---|---|---|---|---|---|---|
| Pb(II) | 0.007(1) | 0.002(1) | 0.030(2) | 0.001(1) | 0 | 0 |
| Ca(II) | 0.007(1) | 0.002(1) | 0.030(2) | 0.001(1) | 0 | 0 |
| Pb(I) | 0.005(3) | 0.005(3) | 0.012(4) | 0.003(2) | 0 | 0 |
| Ca(I) | 0.005(3) | 0.005(3) | 0.012(4) | 0.003(2) | 0 | 0 |
| P | 0.004(6) | 0.005(6) | 0.009(7) | 0.004(5) | 0 | 0 |
| O3 | 0.05(1) | 0.03(1) | 0.01(1) | 0.00(1) | 0.00(1) | −0.001(9) |
| O2 | 0.01(2) | 0.06(3) | 0.01(2) | 0.00(2) | 0 | 0 |
| O1 | 0.02(1) | 0.02(2) | 0.03(2) | −0.001(1) | 0 | 0 |

*Note.* The form of the anisotropic displacement parameter is: $\exp[-2\pi^2\{h^2a^{*2}U(1,1) + k^2b^{*2}U(2,2) + l^2c^{*2}U(3,3) + 2hka^*b^*U(1,2) + 2hla^*c^*U(1,3) + 2klb^*c^*U(2,3)\}]$, where $a^*$, $b^*$ and $c^*$ are reciprocal lattice constants.

**TABLE 4**
**Interatomic Distances (Å) and Angles (°) in LCPbAp Compound**

| | | | | | |
|---|---|---|---|---|---|
| | | *$PO_4$ tetrahedron* | | | |
| P–O1 | 1.55(8) | O2–P–O1 | 109.2(8) | O1–P–O3$s_4$ | 106.5(9) |
| P–O2 | 1.55(3) | O2–P–O3$s_4$ | 114.0(1) | O3–P–O3$s_4$ | 106.0(1) |
| P–O3 | 1.55(1) | O2–P–O3 | 114.0(1) | O1–P–O3 | 106.5(9) |
| P-O3s$_4$ | 1.55(1) | | | | |
| | | Site (II) | | | |
| *M*(II)–O1$s_1$ | 2.300(2) | *M*(II)–O3$s_3$ | 2.52(1) | *M*(II)–O3$s_4$ | 2.58(2) |
| *M*(II)–O3 | 2.58(2) | *M*(II)–O2$s_1$ | 3.39(2) | *M*(II)–O2s$_5$ | 3.09(2) |
| *M*(II)–*M*(II)s$_{10}$ | 4.174(4) | *M*(II)–*M*(II)s$_5$ | 4.174(4) | | |
| | | *Site (I)* | | | |
| *M*(I)–O2$s_6$ | 2.38(2) | *M*(I)–O2s$_7$ | 2.38(2) | M(I)–O2s$_8$ | 2.38(2) |
| *M*(I)–O1 | 2.581(4) | *M*(I)–O1$s_1$ | 2.581(4) | *M*(I)–O1$s_9$ | 2.581(4) |
| *M*(I)–O3 | 2.81(2) | *M*(I)–O3$s_1$ | 2.81(2) | *M*(I)–O3$s_9$ | 2.81(2) |
| *M*(I)–O3s$_9$ | 2.81(2) | *M*(I)–*M*(I)s$_4$ | 3.68(1) | *M*(I)–M(I)s$_{11}$ | 3.44(1) |

*Note*. Symmetry operators: $s_1$: $1-y, x-y, z$; $s_2$: $y, -x+y, 0.5+z$; $s_3$: $y, -x+y, -z$; $s_4$: $x, y, 0.5-z$; $s_5$: $-x+y, -x, z$; $s_6$: $1-x, 1-y, -0.5+z$; $s_7$: $1+x-y, x, -0.5+z$; $s_8$: $y, -x+y, -0.5+z$; $s_9$: $1-x+y, 1-x, z$ $s_{10}$: $-y, x-y, z$; $s_{11}$: $x, y, -0.5-z$.

calculation can give an order of the true Pb-Pb distances in site (I) (Pb(I)–Pb(I) = 3.718 and 3.446 Å).

In the tunnel set around the *c* axis, site (II) is occupied by 4.98 $Pb^{2+}$ and 1.02 $Ca^{2+}$ (Table 2). These cations constitute the walls of the tunnel and are arranged in equilateral triangles (Fig. 4). Their coordination sphere consists of six oxygens pertaining to five $(PO_4)^{3-}$ tetrahedra with an average *M*(II)–O bond length of 2.59(40) Å. Moreover, the *M*(II)–*M*(II) distance in a metal triangle is 4.174(4) Å, a distance close to that found in hydroxyapatite (4.168(1) Å) (32). In the same surrounding, the ionic radius of $Pb^{2+}$ being always greater than that of $Ca^{2+}$ (33), this non variation of *M*(II)–*M*(II) distance may indicate that an interaction between lead atoms may occur stabilizing the structure. A possible overlap of the electron LP of each $Pb^{2+}$ cation can be invoked, leading to an accumulation of electron in the centre of the metal triangle. The stabilization of the apatite-type structure seems to be controlled by the presence of a maximum electron density within these tunnels. These negative charges could be brought either by

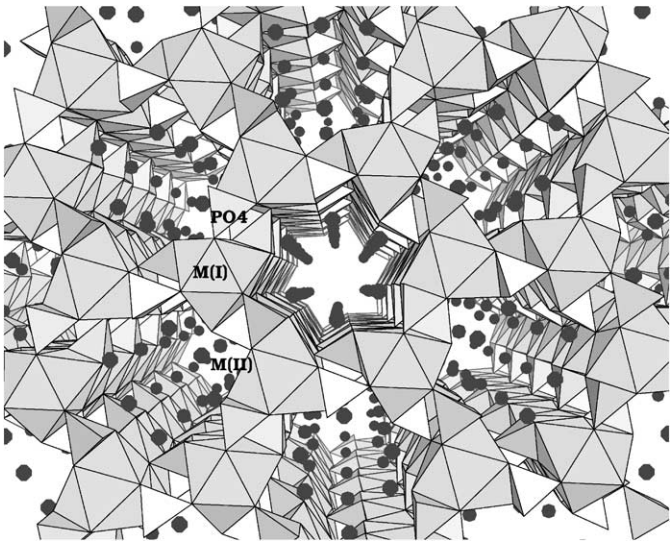


**FIG. 2.** Perspective view of $Pb_6Ca_2Li_2(PO_4)_6$ structure.

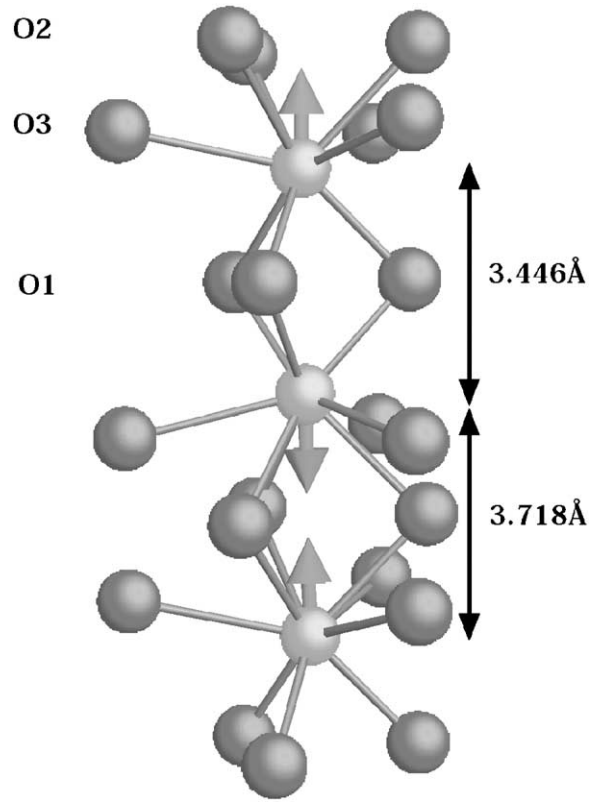


**FIG. 3.** Pb(I)–Pb(I) stacking in $Pb_6Ca_2Li_2(PO_4)_6$ with assumed electron lone pairs orientation.

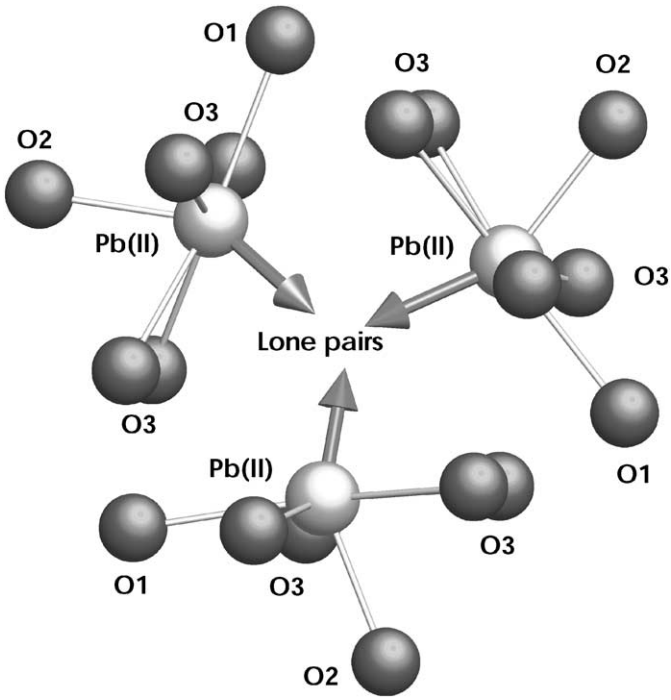


**FIG. 4.** Pb(II)–Pb(II) stacking in $Pb_6Ca_2Li_2(PO_4)_6$ showing a possible arrangment of the electron lone pairs.

distinct anions $Y^{n-}$ ($OH^-$, $F^-$, $Cl^-$, etc) or by electron LPs held by $Pb^{2+}$ cations or other ions such as $Bi^{3+}$ (5, 33). So, such active electron LPs should be considered as a constituent of the coordination spheres of $M$(II) cations, as reported by various authors in different crystalline compounds containing $Pb^{2+}$, $Bi^{3+}$ or $Tl^+$ (3, 4, 33–36). Under these circumstances, the coordination number of M(II) becomes equal to seven as in the $M_{10}(XO_4)_6Y_2$ apatite compounds.

## *Electrical Properties*

The measurements were performed in the temperature range 300–1000 K. Below 700 K the conductivity appears too low to be measured, only impedance diagrams above this temperature are presented in Fig. 5. The resistance was obtained from the intercept of the circle with the real axis. Temperature dependence of the electrical conductivity between 725 K and 900 K is presented in Fig. 6. Because of the high temperature used to understand the conduction process, the conductivity can be attributed to the creation of intrinsic defects such as Frenkel or substitution defects. As demonstrated by Den Hartog *et al.* in fluorapatite (37), the conductivity is dominated by cationic mobility and presents an anisotropy. Conductivity parallel to the *c*-axis is 100 times higher than the perpendicular one.

More recently, Laghzizil *et al.* (17) have studied conductivity in lithium fluorapatites and confirmed that the cationic mobility has a three-dimensional character with elementary jumps between site (I)–site (I), site (II)–site (II) parallel to the c direction and site (I)–site (II) perpendicular to the *c* direction (16, 17, 38). Moreover, they showed that Li compounds are better conductors than Na compounds. In the system $Pb_8K_{2-x}Na_x(PO_4)_6$, Laghzizil *et al.* (15) showed that the disorder defect increases the conductivity and that only $M^I$ cations contribute to the conductivity phenomenon. In our study the activation energy found ($\Delta E_\sigma = 1.05$ eV) is slightly lower than that

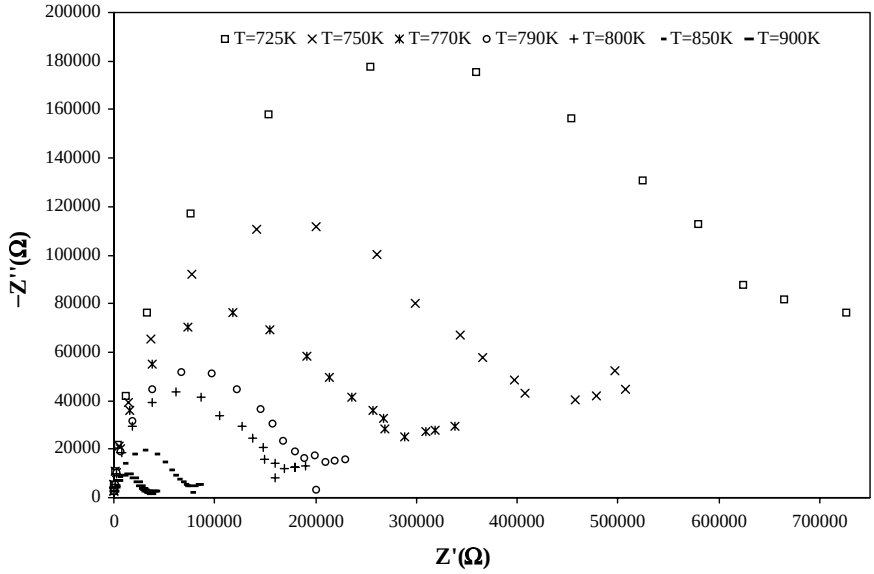


**FIG. 5.** Complex impedance diagrams of $Pb_6Ca_2Li_2(PO_4)_6$ compound.

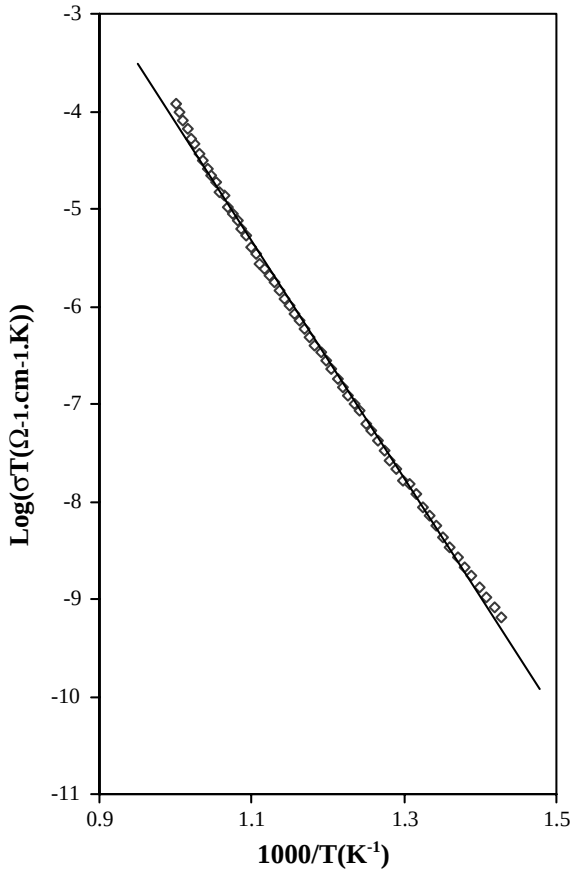


**FIG. 6.** Conductivity plot, Log $(\sigma T) = f(1000/T)$, for $Pb_6Ca_2Li_2(PO_4)_6$.

found in lithium fluorapatite ($\Delta E_\sigma = 1.64$ eV) (17) which confirms that contributions to conductivity of $Ca^{2+}$ and $Pb^{2+}$ are negligible (15).

*Modulus Spectroscopy Analysis*

A plot of Log $M'$ and of the normalized $M''/M''_{max}$ imaginary part of the complex modulus versus Log $f$ is given in Figs. 7 and 8 at various temperatures for the LCPbAp compound. At high frequencies, the value of $M'$ reaches a constant value $M'_\infty$ $(= 1/\varepsilon_\infty)$ whatever the temperature is. At low frequencies it approaches zero, which indicates that the electrode polarization phenomena have a negligible contribution (39). The variation of $M''/M''_{max}$ relative to a given temperature shows an asymmetrical peak approximately centered in the dispersive region (Fig. 8). The left part of the peak corresponds to long-range mobility, the right part of the peak is attributed to ions spatially confined in narrow potential wells. The frequency range where the peak occurs indicates the transition between long- and short-range mobility and is defined by the condition $\omega\iota_\sigma \approx 1$, where $\iota_\sigma$ is the most probable relaxation time of ions (40). The beginning of a second relaxation peak, generally attributed to the grain boundary effects (41), is observable at higher frequency.

With the increase of temperature, the maxima of $M''/M''_{max}$ shift to higher frequencies (Fig. 8). The relaxation frequency ($fp = 1/2\pi\iota_\sigma$) of these maxima corresponds to the bulk relaxation. The temperature dependence of fp is presented in Fig. 9. As expected, fp follows an Arrhenius-type law. Log(σT) is also reported too in Fig. 9 for comparison. Both interpolation lines observed in the temperature range studied are quasi-parallel. Then the activation energies issued from impedance ($\Delta E_\sigma$) and modulus ($\Delta E_f$) spectra are very close ($\Delta E_\sigma = 1.05$ eV; $\Delta E_f = 0.99$ eV), suggesting that the $Li^+$ ion transport in the material is probably due to a hopping mechanism (42). In fact, in LCPbAp Li occupies only site (I), so a unique

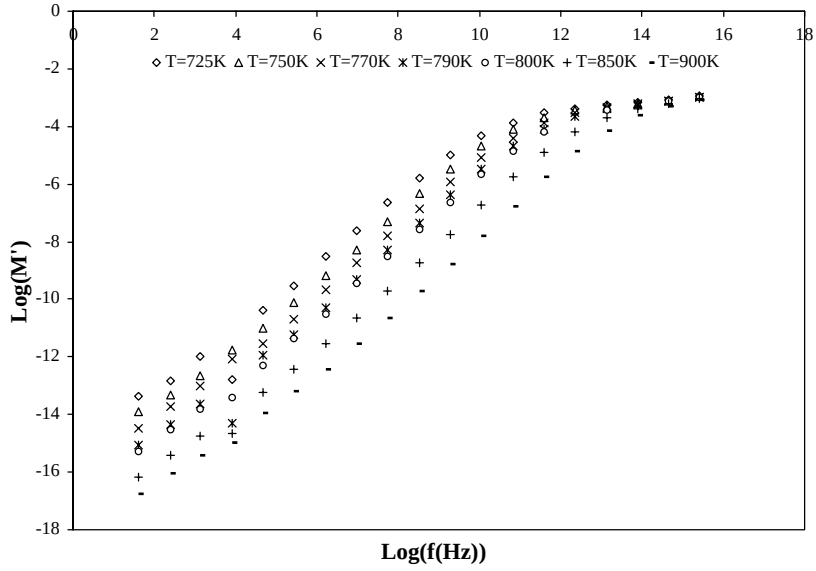


**FIG. 7.** Plots of Log $M'$ versus Log $f$ for $Pb_6Ca_2Li_2(PO_4)_6$ at various temperatures.

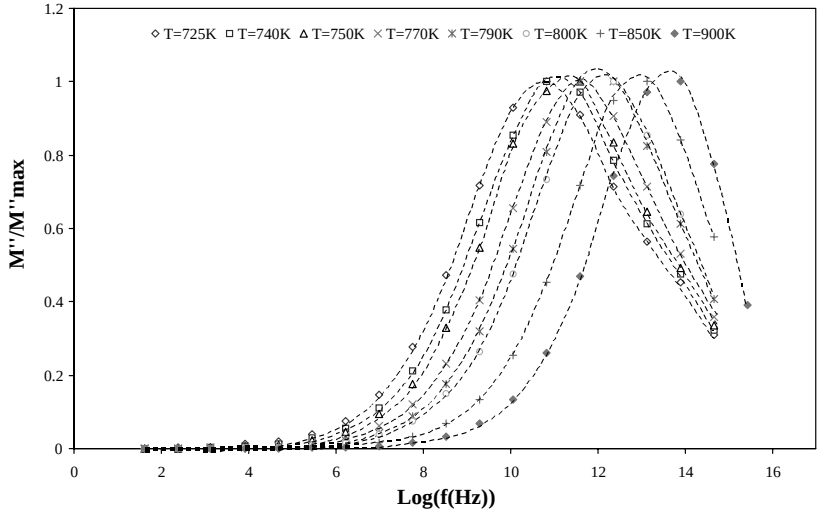


**FIG. 8.** Plots of $M''''/M''_{max}$ versus Log $f$ for $Pb_6Ca_2Li_2(PO_4)_6$ at various temperatures.

type of jump can be expected, i.e., the intra-tunnel jump: site (I)〈—〉 site (I).

## CONCLUSIONS

This paper presents a study of synthesis, characterization and structure determination of a new mixed compound $Pb_6Li_2Ca_2(PO_4)_6$. The X-ray study on a single crystal shows that lithium ions occupy preferentially site (I) and this structure is an anionic lacunary apatite stabilized by the interaction of Pb(II) electron lone pair. The electrical conductivity as a function of temperature can be interpreted assuming a hopping mechanism of Li ions in tunnels.

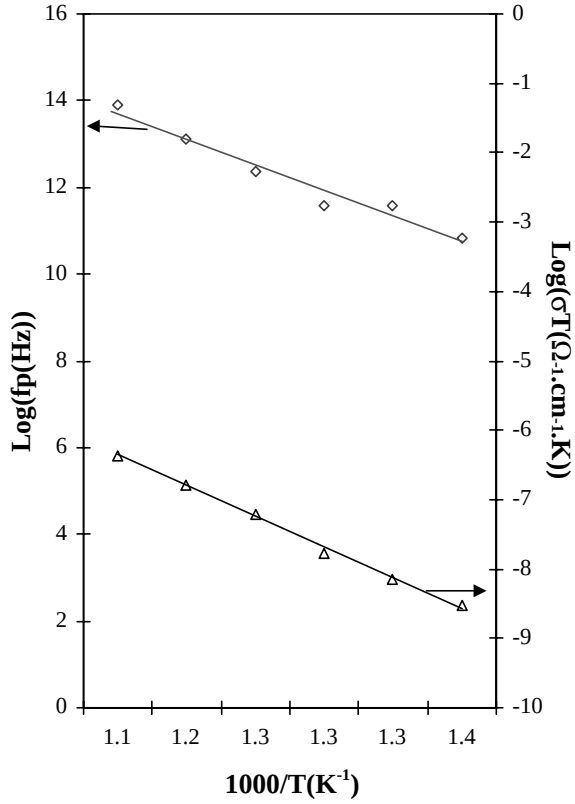


**FIG. 9.** Temperature dependence of Log ($\sigma T$) and Log(fp) for $Pb_6Ca_2Li_2(PO_4)_6$ (fp is the $M''_{max}$ peak frequency at each temperature).

## REFERENCES


1. D. K. Smith, Calcium phosphate in nature, *in* "Hydroxyapatite Related Compounds" (P. W. Brown and B. Constantz, Eds.), pp. 29–44. CRC Press, Boca Raton, FL, 1994.
2. A. Nounah, J. L. Lacout, and J. M. Savariault, *J. Alloys Comp.* **188,** 141 (1992).
3. M. Azzour, L. El Ammari, Y. Le Fur, and B. Elouadi, *J. Solid State Chem.* **141,** 373 (1998).
4. S. P. Sirotinkin, Yu V. Oboznenko, and N. N. Neuskii, *Russ. J. Inorg. Chem.* **34,**1716 (1989).
5. K. H. Butler, "Fluorescent Lamp Phosphors." Pennsylvania State University Press, University Park, PA, 1986.
6. T. S. Davis, E. R. Kreidler, J. A. Parodi, and T. F. Soules, *J. Lumin.* **4,** 48 (1971).
7. J. P. Budin, J. C. Michel, and F. Auzel, *J. Appl. Phys.* **50,** 441 (1979).
8. L. D. Deloach, S. A. Payne, L. L. Chase, L. K. Smith, W. L. Kway, and W. F. Krupke, *IEEE J. Quantum Electron.* **QE-29,** 1179 (1993).
9. S. A. Payne, L. K. Smith, L. D. Deloach, W. L. Kway, J. B. Tassano, and W. F. Krupke, *IEEE J. Quantum Electron.* **QE-30,** 170 (1994).
10. A. O. Wright, M. D. Seltzer, J. B. Gruber, and B. H. T. Chai, *J. Appl. Phys.* **78**(4), 2456 (1995).
11. T. Suzuki, *Gypsum Lim.* **204,** 314 (1986).
12. A. Laghzizil, P. Barboux, and A. Bouhaouss, *Solid State Ionics* **128,** 177 (2000).
13. L. Merker, and H. Wondratschek, *Z. Kristallogr.* **109,** 110 (1957).
14. A. Laghzizil, A. Bouhaouss, M. Ferhat, P. Barboux, R. Morineau, and J. Livage, *Adv. Mater. Res.* **1–2,** 479 (1994).
15. A. Laghzizil, P. Barboux, and A. Bouhaouss, *Solid State Ionics* **128,** 177 (2000).
16. A. Laghzizil, A. Bouhaouss, P. Barboux, R. Morineau, and J. Livage, *Solid State Ionics* **67,** 137 (1993).

17. A. Laghzizil, S. El Hajjaji, A. Bouhaouss, and M. Ferhat, *Solid State Ionics* **126,** 245 (1999).
18. A. Laghzizil, N. El Herch, A. Bouhaouss, G. Lorente, and J. Macquete, *J. Solid State Chem.* **156,** 57 (2001).
19. A. Laghzizil, N. El Herch, A. Bouhaouss, G. Lorente, T. Cordin, and J. Livage, *Mater. Res. Bull.* **36,** 953 (2001).
20. S. Nakayama, M. Sakamato, M. Higuchi, K. Kodaira, M. Sato, S. Kakita, T. Suzuki, and K. Itoh, *J. Eur. Ceram. Soc.* **19,** 507 (1999).
21. G. Engel, *J. Solid State Chem.* **6,** 293 (1973).
22. G. Engel, *J. Solid State Chem.* **6,** 286 (1973).
23. I. Mayer, S. Cohen, and J. R. Matalon, *J. Solid State Chem.* **36,** 271 (1981).
24. M. El Koumiri, S. Oishi, S. Sato, L. ElAmmari, and B. Elouadi, *Mater. Res. Bull.* **35,** 503 (2000).
25. R. Ternane, M. Ferid, M. Trabelsi-Ayedi, and B. Pirou, *Spectrochim. Acta A* **55,** 1793 (1999).
26. R. Ternane, M. Ferid, N. Kbir-Ariguib, M. Trabelsi-Ayedi, *J. Alloys Compd.* **308,** 83 (2000).
27. Chemical analysis performed in the "Service Central d'Analyse du CNRS, Département Analyse Elementaire, 69390 Vernaison, France."
28. G. M. Sheldrick, "SHELXS-86, Program for the solution of crystal structures." University of Göttingen, Germany, 1990.
29. G. M. Sheldrick, "SHELXL-93, Program for crystal structure determination" University of Göttingen, Germany 1993.
30. H. El Feki, T. Naddari, J. M. Savariault, and A. Ben Salah, *Solid State Sci.* **2,** 725 (2000).
31. T. Naddari, H. El Feki, J. M. Savariault, P. Salles, and A. Ben Salah, *Solid State Ionics*, in press.
32. K. Sudarsanan and R. A. Young, *Acta Crystallogr. B* **28,** 3668 (1972).
33. G. Engel, W. Götz, and R. Eger, *Z. Anorg. Allg. Chem.* **449,** 127 (1979).
34. A. Verbaere, R. Marchand,, and M. Tournoux, *J. Solid State Chem.* **23,** 383 (1978).
35. W. H. Baur, *Acta Crystallogr. B* **30,** 1195 (1974).
36. C. Colbeau-Justin, G. Wallez, A. M. Xuriguera, A. Elfakir, S. Jaulmes, and M. Quarton, *Eur. J. Solid State Inorg. Chem.* **34,** 1097 (1997).
37. H. Den Hartog, *Phys. Stat. Sol. B* **53,** 201 (1972).
38. C. Gramer, K. Funke, T. Saatkamp, D. Wilmer, and M. D. Ingram, *Z. Naturforsch*, **50**(a), 613 (1995).
39. F. S. Howell, R. A. Bose, P. B. Maado, and C. T. Moynihan, *J. Phys. Chem.* **78,** 639 (1974).
40. H. K. Patel and S. W. Martin, *Phys. Rev. B* **45,** 10,292 (1992).
41. I. M. Hodge, M. D. Ingram, and A. R. West, *J. Electroanal. Chem.* **74,** 125 (1976).
42. B. V. R. Chowdari and R. Gopalakrishnan, *Solid State Ionics* **23,** 225 (1987).